Synthesis of Soluble and Processable Rod-, Arrow-, Teardrop-, and Tetrapod-Shaped CdSe Nanocrystals

Liberato Manna, Erik C. Scher, and A. Paul Alivisatos*

Contribution from the Department of Chemistry, University of California, Berkeley, California 94720, and Materials Sciences Division, Lawrence Berkeley National Laboratory, University of California, Berkeley, California 94720

Received August 16, 2000

Abstract: The formation of extremely high aspect ratio CdSe nanorods (30:1), as well as arrow-, teardrop-, tetrapod-, and branched tetrapod-shaped nanocrystals of CdSe, has been achieved by growth of the nanoparticles in a mixture of hexylphosphonic acid and trioctylphosphine oxide. The most influential factors in shape control are the ratio of surfactants, injection volume, and time-dependent monomer concentration.

Introduction

The ability to systematically manipulate the shapes of inorganic nanocrystals remains an important goal of modern materials chemistry. The shape and size of inorganic nanocrystals control their widely varying electrical and optical properties.[1−3] One means of achieving shape control is by the use of a static template to enhance the growth rate of one crystallographic face over another. For example, two-dimensional films are obtained when there is favorable epitaxy on a substrate.[4] Pyramidal “dots” are obtained if there is strain between the growing crystallite and the epitaxial substrate, as in the growth of InAs on GaAs[5] and Ge on Si[6−8] or the growth of calcite on carboxyl-terminated lipid bilayers.[9]

There are also many demonstrated cases of anisotropic inorganic nanocrystal growth in liquid media. The vapor−liquid−solid growth mechanism in which a solid rod grows out of a supersaturated droplet has been very successful in creating one-dimensional materials[10] and has been applied to growth of (insoluble) nanorods in a liquid medium.[11,12] Structured reaction media like regular or inverse micelles[13−17] have also been used successfully. An electrochemical method yielded anisotropic gold particles.[18,19] A pronounced effect of the surfactant/precursor ratio on particle shape was observed in the case of platinum nanocrystals.[20] Recently, a new mechanism for the formation of complex nanostructures has been proposed, called “oriented attachment”.[21] In this mechanism, nanocrystals can join together with complete crystallographic alignment and eliminate free surfaces. This mechanism can lead to the formation of many interesting new nanostructures.[21−25]

In this paper, we demonstrate systematic variation of the shape of colloidal semiconductor nanocrystals, using thermal decomposition of organometallic precursors in a hot (∼300 °C) mixture of trioctylphosphine oxide and hexylphosphonic acid.[26] As in the growth of spherical CdSe nanocrystals in hot trioctylphosphine oxide,[27] the surfactants dynamically adsorb to the growing crystallites, allowing atoms to add and subtract for high crystallinity.[28] This enables the growing crystallites to anneal, resulting in good crystallinity, while suppressing particle aggregation. It is important to note that the growth mode of the nanocrystals depends strongly upon monomer concentration.[28] At low monomer concentration, Ostwald ripening occurs, and small nanocrystals dissolve at the expense of larger ones. Such slow growth conditions favor the formation of a spherical particle shape (least surface area). On the other hand, at high monomer concentration, relative differences between the growth rates of different faces can lead to anisotropic shapes. The relative growth rates of the different faces can be controlled by suitable variation of the ratio of trioctylphosphine oxide and

---

(1) Lieber, C. M. *Solid State Commun.* **1998**, *107*, 607−616.
(2) Smalley, R. E.; Yakobson, B. I. *Solid State Commun.* **1998**, *107*, 597−606.
(3) Alivisatos, A. P. *Science* **1996**, *271*, 933−937.
(4) Cho, A. Y. *J. Cryst. Growth* **1999**, *202*, 1−7.
(5) Leon, R.; Petroff, P. M.; Leonard, D.; Fafard, S. *Science* **1995**, *267*, 1966−1968.
(6) Liu, C. P.; Gibson, J. M.; Cahill, D. G.; Kamins, T. I.; Basile, D. P.; Williams, R. S. *Phys. Rev. Lett.* **2000**, *84*, 1958−1961.
(7) Paul, D. J. *Adv. Mater.* **1999**, *11*, 191.
(8) Campbell, S. A. *Mater. Sci. Eng. R−Rep.* **1997**, *20*, 1−36.
(9) Berman, A.; Ahn, D. J.; Lio, A.; Salmeron, M.; Reichert, A.; Charych, D. *Science* **1995**, *269*, 515−518.
(10) Hu, J. T.; Odom, T. W.; Lieber, C. M. *Acc. Chem. Res.* **1999**, *32*, 435−445.
(11) Trentler, T. J.; Hickman, K. M.; Goel, S. C.; Viano, A. M.; Gibbons, P. C.; Buhro, W. E. *Science* **1995**, *270*, 1791−1794.
(12) Holmes, J. D.; Johnston, K. P.; Doty, R. C.; Korgel, B. A. *Science* **2000**, *287*, 1471−1473.
(13) Li, M.; Schnablegger, H.; Mann, S. *Nature* **1999**, *402*, 393−395.
(14) Qi, L. M.; Ma, J. M.; Cheng, H. M.; Zhao, Z. G. *J. Phys. Chem. B* **1997**, *101*, 3460−3463.
(15) Rees, G. D.; Evans-Gowing, R.; Hammond, S. J.; Robinson, B. H. *Langmuir* **1999**, *15*, 1993−2002.
(16) Tanori, J.; Pileni, M. P. *Langmuir* **1997**, *13*, 639−646.
(17) Chen, C. C.; Chao, C. Y.; Lang, Z. H. *Chem. Mater.* **2000**, *12*, 1516−1518.
(18) Chang, S. S.; Shih, C. W.; Chen, C. D.; Lai, W. C.; Wang, C. R. C. *Langmuir* **1999**, *15*, 701−709.
(19) Yu, Y. Y.; Chang, S.; Lee, C. J.; Wang, C. R. C. *J. Phys. Chem. B* **1997**, *101*, 6661−6664.
(20) Ahmadi, T. S.; Wang, Z. L.; Green, T. C.; Henglein, A.; El-Sayed, M. A. *Science* **1996**, *272*, 1924−1926.
(21) Penn, R. L.; Banfield, J. F. *Am. Mineral.* **1998**, *83*, 1077−1082.
(22) Alivisatos, A. P. *Science* **2000**, *289*, 736−737.
(23) Chemseddine, A.; Moritz, T. *Eur. J. Inorg. Chem.* **1999**, 235−245.
(24) Park, S. J.; Kim, S.; Lee, S.; Khim, Z. G.; Char, K.; Hyeon, T. *J. Am. Chem. Soc.* **2000**, *122*, 8581−8582.
(25) Weller, H., personal communication, 2000.
(26) Peng, X. G.; Manna, L.; Yang, W. D.; Wickham, J.; Scher, E.; Kadavanich, A.; Alivisatos, A. P. *Nature* **2000**, *404*, 59−61.
(27) Murray, C. B.; Norris, D. J.; Bawendi, M. G. *J. Am. Chem. Soc.* **1993**, *115*, 8706−8715.
(28) Peng, X. G.; Wickham, J.; Alivisatos, A. P. *J. Am. Chem. Soc.* **1998**, *120*, 5343−5344.

10.1021/ja003055+ CCC: $19.00

hexylphosphonic acid.[26] Using a combination of these parameters, we demonstrate the controlled formation of CdSe nanocrystals with rod, arrow, teardrop, and tetrapod shapes. This wide variation of unusual shapes provides important information about the growth of the nanocrystals.

Experimental Section

I. Materials. Dimethylcadmium ($Cd(CH_3)_2$, 97%) and tri-*n*-butylphosphine ($C_{12}H_{27}P$ or TBP, 99%) were purchased from Strem. $Cd(CH_3)_2$ was vacuum transferred and stored at −35 °C under argon. Selenium (99.999%), tri-*n*-octylphosphine oxide ($C_{24}H_{51}OP$ or TOPO, 99%), and hexylphosphonic dichloride ($C_6H_{13}Cl_2OP$, 95%) were purchased from Aldrich. All solvents used were anhydrous, purchased from Aldrich, and used without any further purification. Hexylphosphonic acid ($C_6H_{15}O_3P$ or HPA) was prepared from hexylphosphonic dichloride according to a standard procedure.[29]

II. Synthesis of CdSe Rods. All manipulations were performed using standard air-free techniques. For the synthesis of CdSe nanocrystal rods, cadmium and selenium precursors were co-dissolved in tri-*n*-butylphosphine and the resulting stock solution was stored in a refrigerator at −20 °C. The solution was quickly removed from the refrigerator and vigorously agitated for 10 s. It was then manually injected, under Ar, via a syringe, into 4 g of a hot (360 °C) binary surfactant mixture of TOPO and HPA. Unless otherwise stated, the above techniques were used in all of the following syntheses.

A. Stock Solutions. Stock solutions were all made in a glovebox under Ar. For stock solution A (molar ratio of Cd/Se of 1.4:1), 0.82 g of $Cd(CH_3)_2$, 1.6 g of Se/TBP (20% Se by weight), and 14.08 g of TBP were stirred for 5 min and then placed in a refrigerator at −20 °C. Stock solution B had a ratio of Cd/Se of 1:1 and was made from 0.82 g of $Cd(CH_3)_2$, 2.27 g of Se/TBP (20% Se by weight), and 13.41 g of TBP. Stock solution C had a ratio of Cd/Se of 1.9:1 and was made from 0.82 g of $Cd(CH_3)_2$, 1.20 g of Se/TBP (20% Se by weight), and 14.48 g of TBP.

B. Surfactant Ratio Experiments. For the low HPA concentration experiment, 3.88 g of TOPO and 0.12 g of HPA were mixed in a three-neck flask under Ar and then heated to 360 °C with constant stirring. This mixture is 3% HPA by weight and 8% by molar concentration. The medium concentration experiment was 8% HPA by weight (20 mol %), and used 3.68 g of TOPO and 0.32 g of HPA. The high concentration experiment was 20% HPA by weight (58 mol %) and used 3.20 g of TOPO and 0.80 g of HPA. Henceforth, all concentrations of HPA in TOPO are given in molar concentrations, unless otherwise stated.[30] For each of these experiments, 2.0 mL of stock solution A was injected into solution at a rate of ~20 mL/s. Aliquots were taken at 4, 10, and 30 min after the injection. The reactions were stopped after 30 min by quenching the solution with toluene. These experiments were repeated three times each. The temperature drop observed during rod experiments was from 360 to ~300 °C, and the temperature was maintained at 300 °C unless otherwise stated.

C. Injection Volume Experiments. All injection volume experiments were performed by injecting stock solution A into a 20 mol % solution of HPA in TOPO at 360 °C. The largest volume injection experiment was performed by injecting 2.0 mL of stock solution in less than 0.2 s.[28] In other experiments, 1.5 and 1.0 mL of stock solution were injected into the surfactant mixture using the same amount of time per injection.

D. Multiple Injection Experiments. Multiple injection experiments were performed using all three stock solutions, with up to four additional injections for each stock solution. All experiments were performed in 20 mol % HPA in TOPO at 360 °C. The following experimental procedure is given for the medium rods pictured in this paper. For longer or shorter rods, additional or fewer injections were used, respectively. First, 2.0 mL of stock solution B was injected at a rate of 20 mL/s. After waiting 1 min and 40 s, an additional 1.5 mL of stock solution B was injected dropwise over 6 min and 20 s. The synthesis was stopped 27 min after completion of the injection. For the longest rods, four additional slow injections were performed after the initial nucleation injection. Each of these injections used 1.0 mL of stock and was injected over a period of 6 min. The wait time between slow injections was 10 min, and the reaction was stopped 1 h after the fourth slow injection was finished.

E. Ripening Experiment. To form teardrop particles, 1.0 mL of stock solution A was injected into 20% HPA in TOPO at 360 °C at a rate of 10 mL/s. The temperature was kept at 328 °C. The high temperature and low monomer concentration promoted Ostwald ripening of the nanocrystals. An additional slow injection of 2.0 mL of stock solution A was started after 1 min. This injection took 4 min. The synthesis was stopped 20 min after completion of the slow injection.

III. Shape Selective Dissolution and Precipitation. When the syntheses described above yielded monodisperse samples (both size and shape), no further size selection was applied. If a distribution of lengths and shapes was observed, the following procedure was used to separate them. Methanol was added to the nanocrystal solution until the nanocrystals all precipitated. This precipitate was washed twice with methanol to remove residual TOPO, TBP, and HPA and was redissolved in toluene. This solution was centrifuged for 30 min. If a precipitate (1) appeared at the bottom of the vial, the supernatant (2) was transferred in another vial and the precipitate (1) was dissolved in chloroform. This solution (1) contained the longest rods. In the case of long rods (40 nm or longer), not all the precipitate was soluble in chloroform and the dispersion became clear only after the addition of a small amount of dodecylamine (1−2 mg for a 100-mg precipitate). To the supernatant (2), methanol was added dropwise while under constant agitation, until the solution became cloudy. The solution was then centrifuged and the precipitate (3) was dissolved in toluene or chloroform. This procedure was repeated, obtaining shorter rods and tetrapods in each subsequent precipitate. In all of the above cases, the final product is filtered through a 0.2-μm PTFE filter to remove any nonnanoscale materials that might be present.

IV. Characterization of Samples. A. UV−Visible Absorption Spectroscopy. Absorption spectra were measured using a Hewlett-Packard 8453 UV−visible diode array spectrometer equipped with a deuterium lamp having a resolution of 2.0 nm. A small amount of sample (~10 μL) was removed via syringe and diluted to an optical density of between 0.1 and 0.5 by addition of either toluene or chloroform. The exciton peak in the absorption spectrum taken immediately after injection is broad and between 600 and 620 nm. If monitored throughout the growth, the exciton peak blue-shifts to around 560 nm and then narrows. This happens because upon injection there is a broad size distribution of rod lengths. As the rods grow longer the long axis grows beyond the confinement regime, and the exciton peak only depends on the short axis (diameter) of the rods. Unlike typical nanocrystal synthesis where the peak red-shifts as the size increases,[31] the rods blue-shift, since as the length increases beyond the confinement regime, the exciton peak is only dependent on the short axis. The short axis (3−4 nm) is smaller than the rods were initially long, so the exciton peak blue-shifts even though the rods increase in length.

B. Transmission Electron Microscopy (TEM). Nanocrystal size, morphology, and structure were measured by TEM at the National Center for Electron Microscopy at Lawrence Berkeley Laboratory, on a Topcon EM002B electron microscope. The microscope was operated at an accelerating voltage of 120 kV to minimize beam damage to the sample.

Nanocrystals were deposited from dilute solution onto a 3−4-nm-thick film of amorphous carbon supported by a 400-mesh copper grid (purchased from Ted Pella). One drop of nanocrystal solution in either toluene or chloroform was deposited onto the grid and allowed to evaporate. The sample was then washed with methanol to remove excess organic compounds and placed in a vacuum desiccator overnight.

Structural determination and observation of stacking faults was accomplished using high-resolution TEM (HRTEM) at 440000× magnification. Average sizes and morphologies were measured at 88000× magnification, calibrated using known crystal lattice spacings measured at higher magnifications. Average lengths and shape distributions were determined by counting at least 300 nanocrystals per sample for statistical purposes.

---

(29) Andriano. Ka; Vasileva, T. V.; Demykina, T. K. *Zh. Obshch. Khim.* **1970**, *40*, 1565.

(30) All HPA concentrations given in ref 26 were given by weight.

(31) Alivisatos, A. P. *J. Phys. Chem.* **1996**, *100*, 13226−13239.

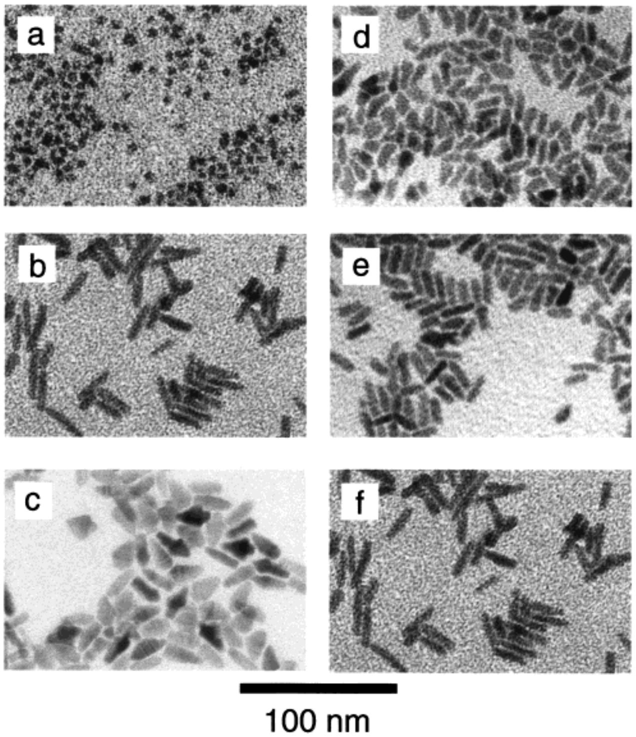

Figure 1. TEMs of the single-injection experiments. All of the surfactant ratio experiments (a−c) used an injection volume of 2.0 mL of stock solution. The surfactant ratio was increased from (a) 8 to (b) 20 to (c) 60% HPA in TOPO. For the injection volume experiments (d−f), 20% HPA in TOPO was used, as it was found to provide optimal rod growth conditions. The injection volumes used were (d) 1.0, (e) 1.5, and (f) 2.0 mL. Greater injection volume favors rod growth (d−f).

C. Powder X-ray Diffraction (XRD). Powder XRD was performed on a Bruker-AXS D8 general area detector diffraction system (GADDS), using Co Kα radiation (1.790 26 Å). Two-dimensional patterns were angle integrated to obtain the patterns displayed. The instrument resolution is 0.07° in 2θ, and the accumulation time for each sample was at least 20 min. The 2θ range used was from 20 to 65° (Q = 1.5−4.0 Å^{-1}, $Q = (4\pi \sin \theta)/\lambda$) at an Ω angle of 15°. XRD samples were prepared by evaporating several drops of a nanocrystal solution on a quartz plate. Prior to the measurements, the samples were washed with methanol to remove excess organic material and dried.

XRD sizing of particles was performed using the Debye−Scherrer equation.[32] The (002) peak at Q = 1.8 Å^{-1} was used to determine the length of the crystalline domain along the long axis of the rods. Peaks were fit using commercial software (PeakFit v4) utilizing a Gaussian−Lorentzian peak shape. The instrument broadening was measured using bulk LaB_6 and then subtracted using a standard correction[32] to the Debye−Scherrer equation.

Results

In this study of the influence of synthesis conditions on the shape of CdSe nanoparticles, three fundamental parameters were varied: the ratio of the surfactants (HPA/TOPO); the volume of the initial injection; and the time dependence of the monomer concentration.

Rods and Arrows: Surfactant Ratio and Injection Volume. For fixed injection conditions, variations of the TOPO/HPA ratio systematically control the nanocrystal shape, as is clearly seen in the low-resolution TEM images in Figure 1a−c and Table 1. With no HPA and at low concentrations of HPA (less than 10%), roughly spherical dots are formed, as previously demonstrated[26] (see Figure 1a). At HPA concentrations of 20%, high aspect ratio rod growth is strongly favored (see Figure 1b). Finally, if the HPA concentration is ∼60%, nanocrystals shaped like arrows are obtained (Figure 1c and Figure 2 a). This can be more clearly seen in the HRTEM images in Figure 2b−e. We observe nanocrystals that look like pencils (Figure 2b), arrows (Figure 2c), and pine trees (Figure 2d,e), as well as rods. The time dependence of the shape composition of the nanocrystals and the average lengths is given in Table 2. The amount of arrow- and tree-shaped nanocrystals increases with time as the amount of rod- and pencil-shaped nanocrystals decrease. The average lengths of the long axis (c-axis) of the different shapes of particles within each sample are within 2% of each other.

Table 1

HPA concn (mol %)	injection vol (mL)	length (nm)	aspect ratio (c:a)
8	2.0	5.1 ± 0.8	1:1
20	2.0	21.8 ± 4.2	5:1
60	2.0	21.7 ± 2.0	varies
20	1.0	13.0 ± 2.1	2:1
20	1.5	16.4 ± 1.1	2.7:1
20	2.0	21.8 ± 4.2	5:1

Variation of the injection volume plays an important role in determining the shape of the nanocrystal. All initial injections are performed in the same amount of time, which is less than 0.2 s. At an HPA concentration of 20%, previously determined to be optimal for nanorod formation, we can observe the effect of varying the injection volume in Figure 1d−f. As the injection volume increases from 1.0 to 1.5 to 2.0 mL, the rods become progressively longer with higher aspect ratio as seen in Table 1.

Extended Rods via Multiple Injections. The longest and highest quality (closest to perfect wurtzite structure) nanorods are obtained using 20% HPA, an initial injection volume of 2.0 mL, and then a slow addition of monomer to sustain growth of the $(00\bar{1})$ face without any additional nucleation (Figure 3). In this manner, rods exceeding 100 nm in length and aspect ratio of over 30:1 have been obtained. The degree of control over rod length and aspect ratio can be seen in Figure 4. Panels a, d, and g of Figure 4 are low-resolution TEM, powder XRD, and HRTEM of a 5.5:1 aspect ratio quantum rod sample, respectively. In Figure 4d, we see an XRD pattern representative of a typical CdSe nanorod sample with wurtzite structure. It is distinguished by the sharp (002) peak, which results from the extended crystalline domain along the c-axis of the wurtzite lattice. The average lengths and aspect ratios of the short, medium, and long rods are presented in Table 3. The discrepancy between TEM and XRD sizing comes about because stacking faults broaden the XRD peak width[32] (therefore making the size appear smaller), while with TEM sizing one measures the entire length of each particle directly. The HRTEM image in Figure 4g is representative of the rods produced in this sample and shows the nearly perfect wurtzite structure of the rods. The medium-length rods in Figure 4b have an aspect ratio of 11:1. The difference between the measured length via TEM and the calculated length from XRD increases with nanocrystal size, implying the presence of more stacking faults in the longer rods. In the HRTEM of the very long rods (Figure 4h), it is observed that there are significant numbers of stacking faults present in the long rod sample. Stacking faults in the wurtzite structure are equivalent to alternating layers of wurtzite (ABAB stacking) and the closely related zinc blende structure (ABCABC stacking) as illustrated in Figure 5. In the powder XRD pattern of the

---

(32) Guinier, A. *X-ray Diffraction In Crystals, Imperfect Crystals, and Amorphous Bodies*; Dover: New York, 1994.

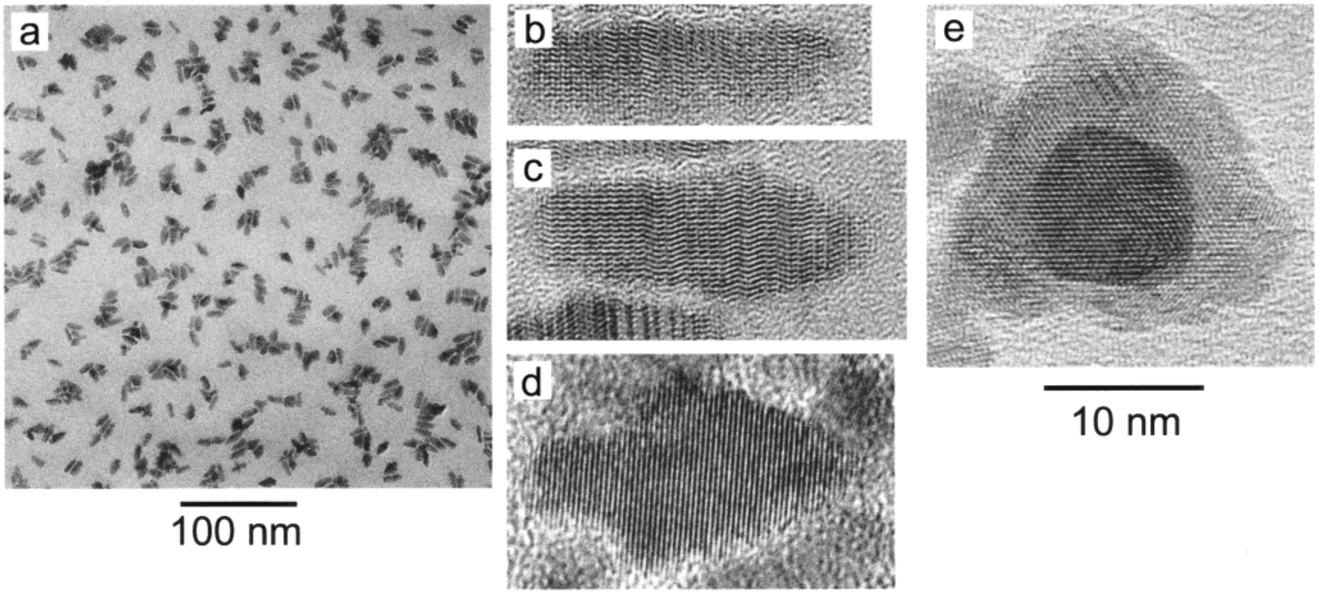

Figure 2. TEMs of a typical 60% HPA concentration sample, showing (a) arrow-shaped nanocrystals. HRTEM images show the stages of growth from (b) pencil- to (c) arrow- to (d) pine tree-shaped nanocrystals. (e) A pine tree-shaped nanocrystal is also shown looking down the [001] direction (or long axis). HRTEM characterization shows that each shape of nanocrystal is predominately wurtzite and that the angled facets of the arrows are the (101) faces.

Table 2

time (min)	length (nm)	rod/pencil (%)	arrow/tree (%)
4	21.7 ± 2.0	56	44
10	27.4 ± 3.0	37	63
30	31.6 ± 3.4	35	65

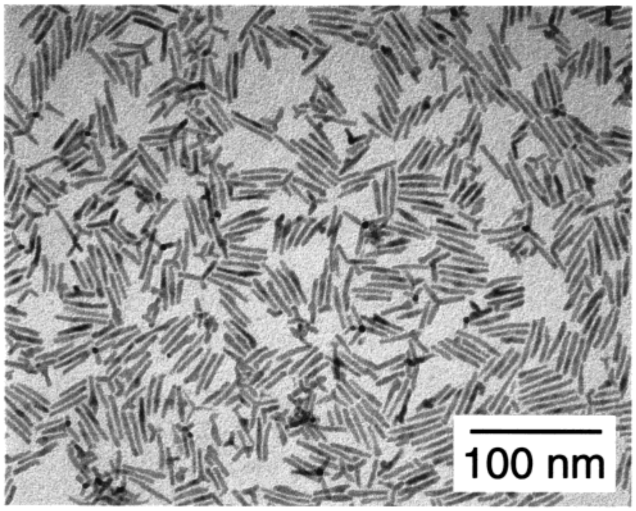

Figure 3. TEM of a typical multiple injection extended rod synthesis. The average length is 34.5 ± 4.4 nm with an aspect ratio of 10:1. The sample contains less than 5% tetrapods.

long rods (Figure 4f), the increase in the amount of zinc blende layers is observed as the relative ratio of the peaks at $Q = 3.0$ and 3.5 $Å^{-1}$ (which correspond to diffraction peaks in both wurtzite and zinc blende) to the wurtzite (103) peak at $Q = 3.2$ $Å^{-1}$ increases, as compared with the shorter rods in Figure 4d. In HRTEM, the change in structure can be observed directly. Wurtzite appears as a characteristic zigzag structure when viewed down the [100] direction, as seen in the short rod (Figure 4g), while zinc blende does not. In Figure 4h, both wurtzite and zinc blende layers are observed within the longest nanocrystals, examples of which are indicated by the regions marked “wur” for wurtzite and “zb” for zinc blende.

Teardrops. More complex variations of the monomer concentration versus time can be used to create unusually shaped nanocrystals and, at the same time, lend considerable insight into the growth mechanism. One procedure used was to grow nanocrystals with a slow injection rate (1.0 mL/s), which results in a drop of the monomer concentration below the Ostwald ripening limit for some time. At this point, the nanocrystals will form low aspect ratio rods or, if left under these conditions for a considerable amount of time, nearly spherical dots. As a next step, the monomer concentration was once again increased with an additional slow injection to reinitiate rod growth. From Figure 6a,b, it appears that particle growth occurs selectively on one crystal face of the rods, thus forming almost teardrop-shaped particles. There are exceptions, as can be seen in Figure 6c, which shows a particle with growth occurring on two faces. Characterizing these cases with HRTEM revealed that they represent nanocrystals with largely zinc blende structure, a defect, or a combination of the two. All crystals that were pure wurtzite grew significantly more on the $(00\bar{1})$ face of the nanocrystal, forming teardrops.

Tetrapods. Another nanocrystal shape that can be consistently obtained is tetrapod nanocrystals as seen in Figure 7a. There are lattice fringes throughout the crystal, indicating crystallinity in both the center and the arms. These shapes are observed in all the syntheses that lead to rod formation and are selected out via size/shape-selective precipitation as detailed in the Experimental Section. Tetrapods typically constitute 15−40% of all particles in the initial sample depending on the growth conditions. After size/shape selection, tetrapods make up less than 5% of the first precipitate and are mainly contained in the second or third fractions isolated. When additional injections into solutions containing tetrapods are performed, “dendritic” tetrapods can be formed as seen in Figure 7b. Up to three additional “branches” can be grown off the end of each arm of the tetrapod.

Discussion

The diverse range of observed shapes can be understood as arising from three basic effects: the nanocrystals will eventually

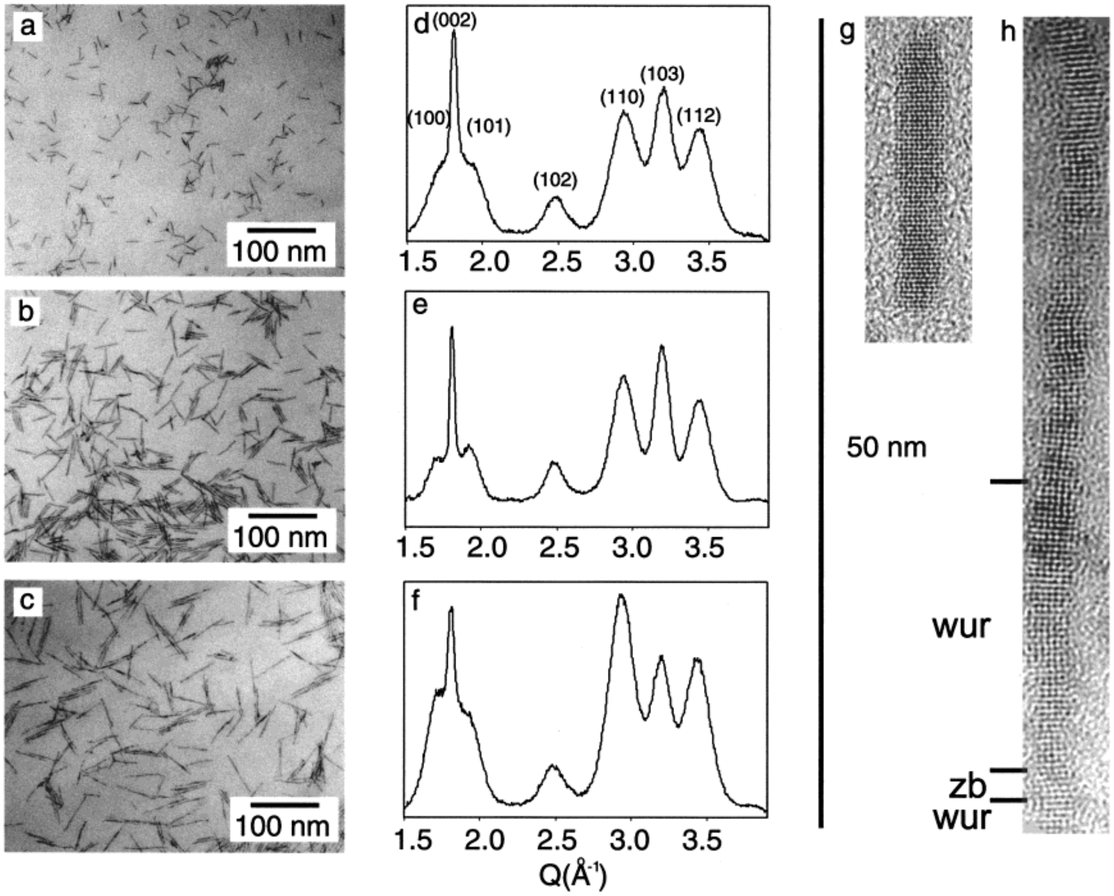

Figure 4. Multiple injection experiments were characterized by TEM, powder XRD, and HRTEM. TEM images of (a) short rods (5.5:1 aspect ratio), (b) medium rods (11:1 aspect ratio), and (c) long rods (20:1−30:1 aspect ratio) show the increase in length. This is verified by (d−f) powder XRD of the same samples. HRTEM images of (g) short rods and (h) long rods demonstrate the increase in the number of stacking faults (and hence zinc blende) present as the size increases. The HRTEM image (g) of the short rod is all wurtzite, while the image (h) of the long rods clearly has different crystal regions present. A few layers of wurtzite (wur) and zinc blende (zb) are denoted in the figure.

Table 3

rods	length (nm) TEM	length (nm) XRD	aspect ratio (c:a)
short	19.6 ± 2.0	17.8	5.5:1
medium	32.8 ± 2.0	26.5	11:1
long	65.8 ± 8.9	32.5	20:1−30:1

tend toward nearly spherical shapes at slow growth rates; rods form at high growth rates by unidirectional growth of one face; HPA accentuates the differences in the growth rates among various faces.

Large injection volume or very high monomer concentration favors rod growth**.** This is clearly seen in the experiments where the injection volume is systematically increased. As the volume injected increases, the nanocrystal rods become progressively longer. Larger injections guarantee that the monomer concentration will be higher in the period of time just after nucleation. When the concentration of monomer present just after nucleation is high, the difference in growth rates between the unique *c*-axis of the wurtzite crystal and the other axes is accentuated, and rods are obtained.

The role of HPA seems to be to increase the growth rate of the $(00\bar{1})$ face of CdSe *relative* to all other faces. This can be seen from the experiments where the injection volume is held constant and the HPA/TOPO ratio is increased. At low concentrations of HPA, spherical-shaped nanocrystals form. Intermediate amounts of HPA favor the formation of rods. It is possible to keep the monomer concentration high by making multiple injections, and thus to prolong the rod growth, yielding rods in excess of 100 nm in length. The diameters of these rods are still determined by the injection step, where size distribution focusing can be used to keep the distribution tight.[28]

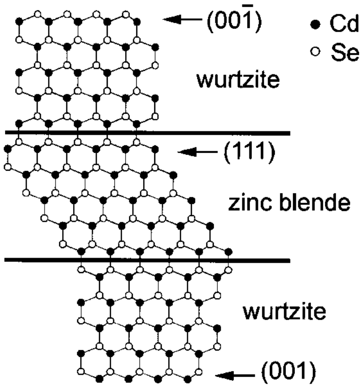

Figure 5. Two-dimensional representation showing the relationship between the wurtzite and zinc blende structures. Wurtzite has ABAB stacking while zinc blende has ABCABC stacking. The (111) face of zinc blende and the $(00\bar{1})$ face of wurtzite both have planes alternately composed of Cd and Se atoms. The two structures are related by a stacking fault.

Higher HPA ratios naturally lead to the formation of arrow-shaped nanocrystals. This can be understood as arising from further enhancement of the growth rate of the $(00\bar{1})$ face relative

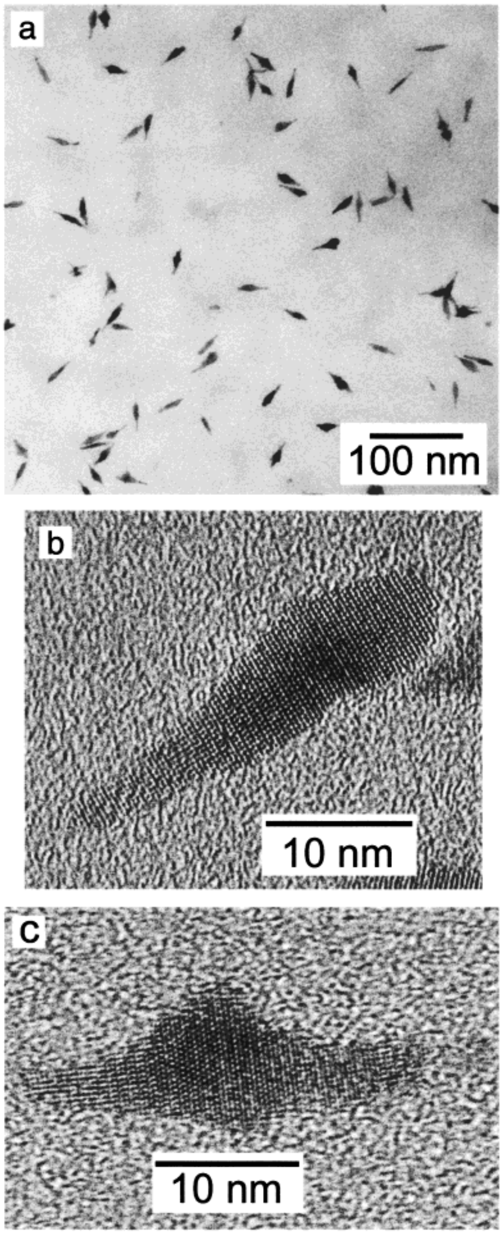

Figure 6. TEMs of (a) typical teardrop-shaped nanocrystals. A HRTEM image (b) shows the wurtzite structure of particles that are teardrop shaped. A HRTEM image (c) of a nanocrystal, which after an additional injection, shows growth on both the (001) and $(00\bar{1})$ faces. The center of this particle is zinc blende in structure. Particles demonstrating growth on both faces make up a very small portion of the observed nanocrystals.

to the other faces. In crystal growth, the fastest growing face is eventually replaced by slower growing faces,[33] and this is how the basic arrow shapes in Figure 2b−e arise. The {101} faces of the arrow grow more slowly than the $(00\bar{1})$ face, and in the high HPA limit where $(00\bar{1})$ is growing extremely quickly, it is eventually replaced by the (101) equivalent faces. Within the kinetic regime, these variations of shape will arise just from differential growth rates of the various faces, regardless of absolute rate of growth (whether the growth of the unique face is enhanced or the growth rates of all the other faces are retarded by the HPA).

The wide variety of shapes observed in the high HPA concentration sample is a result of capturing the nanocrystals in different stages of their growth. Using TEM images of samples taken at different times after injection, we can follow the shape evolution as the reaction proceeds. The percentage of arrow- and tree-shaped nanocrystals increases with time while the amount of rods and pencils decreases. Despite the fact that the nanocrystals presumably grow from rods to pencils to arrows to pine trees, the rate of growth of the $(00\bar{1})$ face is nearly constant. The average lengths of different particle shapes at a certain time agree to within 2% of each other, indicating that the rate of growth along the *c*-axis is not affected by the additional growth on the sides of the nanocrystal.

The formation of arrows unequivocally points to *unidirectional growth*. The hexagonal CdSe nanocrystals do not have inversion symmetry, meaning the top and bottom faces of the crystals are intrinsically different. As can been seen in Figure 8, Cd atoms on the (001) face have one dangling bond, while Cd atoms on the $(00\bar{1})$ face have three dangling bonds. It appears that, in the presence of HPA, the relative growth rate of the $(00\bar{1})$ face is much greater than that of the others.

Teardrop growth illustrates nicely the concept of time variation of monomer concentration as a means of deliberately creating nanocrystals with complex shapes. The unidirectional growth noted in arrow formation is also a factor in the formation of the teardrops. Here, however, we take advantage of the third major effect, namely, that slow growth favors equilibrium, round shapes. Teardrop shapes arise when rodlike crystals are subsequently grown at low monomer concentration and slow injection volume, and then the monomer concentration is abruptly increased. The rods first become rounded, forming the body of the tear, and then when the monomer concentration is increased, the droplet elongates.

Further support for the argument that HPA increases the relative growth rate of only the $(00\bar{1})$ face of hexagonal CdSe comes from the formation of tetrapod-shaped nanocrystals. These are remarkable single-crystal particles consisting of a tetrahedral zinc blende core with four wurtzite arms. Epitaxial growth of wurtzite layers out of a tetrahedral zinc blende core has been observed before.[34] Like the {001} planes of the wurtzite structure, the {111} planes of the zinc blende structure contain layers alternately composed of either Cd or Se as can be seen in Figure 5. Since the presence of HPA selectively increases the growth rate of the $(00\bar{1})$ face, it follows that the closely related zinc blende {111} faces would also grow quickly in this binary surfactant mixture. The tetrapods are formed when a CdSe nanocrystal nucleates in the zinc blende structure instead of the wurtzite structure. Then wurtzite arms grow out of the four (111) equivalent faces of the tetrahedral zinc blende core as seen in Figure 9. There may be several ways of selectively adjusting the relative amounts of zinc blende versus wurtzite nuclei formed in the injection process. Similar structures are observed on a larger length scale in zinc oxide,[35−37] though the growth mechanism is not comparable, since they are not prepared in solution.

More complex shapes, such as dendritic tetrapods, are produced by performing additional injections of monomer into a solution already containing tetrapods. Growth occurs at the ends of the tetrapod arms with each additional injection. If the arms are purely wurtzite, they will continue to grow straight. If

---

[33] Brice, J. C. *The Growth of Crystals from Liquids*; North-Holland Pub. Co.: Amsterdam, 1973.

[34] Mews, A.; Kadavanich, A. V.; Banin, U.; Alivisatos, A. P. *Phys. Rev. B: Condens. Matter Mater. Phys.* **1996**, *53*, 13242−13245.

[35] Ataev, B. M.; Kamilov, I. K.; Mamedov, V. V. *Tech. Phys. Lett.* **1997**, *23*, 842−843.

[36] Satoh, M.; Tanaka, N.; Ueda, Y.; Ohshio, S.; Saitoh, H. *Jpn. J. Appl. Phys. Part 2.* **1999**, *38*, L586−L589.

[37] Zhou, Z. W.; Deng, H.; Yi, J.; Liu, S. K. *Mater. Res. Bull.* **1999**, *34*, 1563−1567.

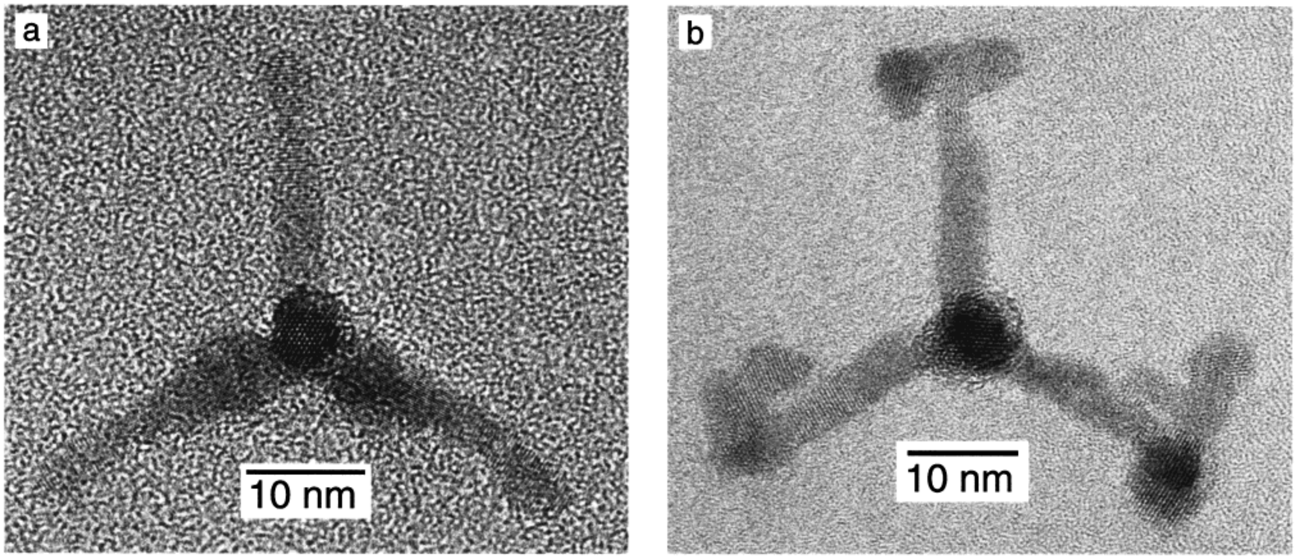

Figure 7. HRTEM image (a) of a typical tetrapod-shaped CdSe nanocrystal, looking down the [001] direction of one arm. Lattice spacings confirm that all four arms are of the wurtzite structure. In image b, we see a tetrapod that has branches growing out of each arm. There are zinc blende layers near the ends of the original arms, and the branches are wurtzite with some stacking faults.

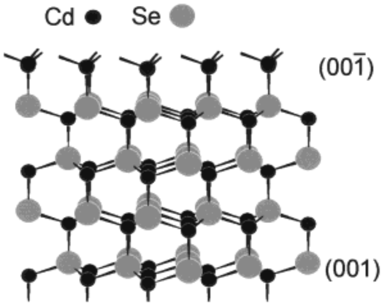

Figure 8. Atomic model of CdSe in the wurtzite structure demonstrating the differences between the (001) and $(00\bar{1})$ faces. On the (001) face, Cd atoms have only one dangling bond, while on the $(00\bar{1})$ face Cd atoms have three dangling bonds that need to be passivated.

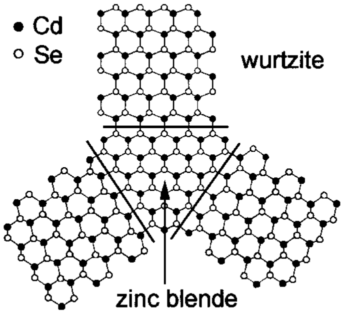

Figure 9. Two-dimensional representation showing the structure of a tetrapod. The nuclei is the zinc blende structure, with wurtzite arms growing out of each of the four (111) equivalent faces. Three are shown, with the fourth coming out of the page toward the reader.

there are zinc blende layers or stacking faults near the end of the arms, which is a statistical probability, multiple (up to three maximum) additional "branches" will grow out of each arm. This can be clearly seen in Figure 7b, where a second injection has been performed on a sample containing tetrapods.

To this point, we have not assigned a microscopic mechanism by which the HPA acts upon the different faces. All of the effects described above can be explained by modulation of the relative growth rates of the different faces, but the microscopic mechanism is of course of great interest. We believe that it is less likely that "oriented attachment"[21] of nanocrystals is operative here. This mechanism would have difficulty accounting for the arrow-shaped nanocrystals, as the "shaft" of the arrow is always centered on the "arrowhead", there is only one shaft per arrowhead, and the lengths of all the different shapes encountered are very close to each other. This would require the separate components (presumably arrowhead and shaft) to attach only after growing to a certain length or would require a concerted attachment mechanism throughout the solution. Previously, oriented attachment has only been observed in systems where the nanocrystals are coated with small molecules that allow the nanocrystals to get close to each other and even facilitate attachment[21,25] In our system, however, the CdSe nanocrystals are coated with long-chain organic molecules that would hinder the nanocrystals from attaching to each other. At this point we can make two hypotheses about the possible growth mechanism occurring in our system. One is that the HPA, protonated or deprotonated, may act as surfactant directly, adsorbing, for instance, to the (001) face and to the {110} faces and shutting down the growth on these faces. Alternatively, the highly acidic environment may influence the growth rates by protonation of particular faces. Not much is known about the complex reaction mixture of TOPO and HPA at such elevated temperatures, and this will be the subject of intensive future study.

Acknowledgment. This work was supported by the National Science Foundation (Grant DMR-9726597), Lawrence Livermore National Labs (Contract W-7405-Eng-48), and the Director, Office of Energy Research, Office of Science, Division of Materials Sciences, of the U.S. Department of Energy under Contract DE-AC03-76SF00098. We thank the National Center for Electron Microscopy for the use of their TEMs and computing facilities, especially Chris Nelson for his help and support. Thank you to Dr. Fabio Zürcher for assistance with the diffractometer and Dr. Jörg Rockenberger and Stephen Prilliman for many helpful discussions.

JA003055+